Journal of Computational Physics 369 (2018) 237–251

Contents lists available at ScienceDirect

Journal of Computational Physics

www.elsevier.com/locate/jcp

A heterogeneous FMM for layered media Helmholtz equation I: Two layers in $\mathbb{R}^2$

Min Hyung Cho [a], Jingfang Huang [b], Dangxing Chen [b], Wei Cai [c,*]

[a] Department of Mathematical Sciences, University of Massachusetts Lowell, Lowell, MA 01854, USA
[b] Department of Mathematics, University of North Carolina at Chapel Hill, Chapel Hill, NC 27599, USA
[c] Department of Mathematics, Southern Methodist University, Dallas, TX 75275, USA

ARTICLE INFO

Article history:
Received 12 October 2017
Received in revised form 29 March 2018
Accepted 4 May 2018
Available online 9 May 2018

Keywords:
Helmholtz equation
Impedance boundary condition
Fast multipole method
Hierarchical model
Low-rank representation
Multi-layered media

ABSTRACT

In this paper, we introduce a new heterogeneous fast multipole method (H-FMM) for 2-D Helmholtz equation in layered media. To illustrate the main algorithm ideas, we focus on the case of two layers in this work. The key compression step in the H-FMM is based on a fact that the multipole expansion for the sources of the free-space Green's function can be used also to compress the far field of the sources of the layered-media or domain Green's function, and a similar result exists for the translation operators for the multipole and local expansions. The mathematical error analysis is shown rigorously by an image representation of the Sommerfeld spectral form of the domain Green's function. As a result, in the H-FMM algorithm, the multipole-to-multipole, multipole-to-local, and local-to-local translation operators are the same as those in the free-space case, allowing easy adaptation of existing free-space FMM. All the spatially variant information of the domain Green's function is collected into the multipole-to-local translations and therefore the FMM becomes heterogeneous. The compressed representation further reduces the cost of evaluating the domain Green's function when computing the local direct interactions. Preliminary numerical experiments are presented to demonstrate the efficiency and accuracy of the algorithm with much improved performance over some existing methods for inhomogeneous media.

1. Introduction

To compute the interactions of the electromagnetic or acoustic waves with objects of complex geometry embedded in multi-layered media, an attractive numerical method in the engineering community is to reformulate the frequency domain Helmholtz equation as integral equations using the *layered-media Green's function* where the unknowns are only defined on the surface or volume of the objects [1–4]. In contrast, integral equation methods based on the *free-space Green's function* require unknowns and equations on the infinite interfaces of the background layered-media. Unlike the translation-invariant free-space Green's function for wave scattering in homogeneous media, the layered-media Green's function incorporates the interface and far-field boundary conditions and becomes a spatially variant function. In this work, we will refer to the layered-media Green's function as the domain Green's function or domain kernel function. Subsequently, the boundary or volume integral equations are discretized using proper numerical integration techniques, for instance, the

* Corresponding author.
E-mail address: cai@smu.edu (W. Cai).

https://doi.org/10.1016/j.jcp.2018.05.007
0021-9991/

trapezoidal rule with end point corrections [5,6] in two dimensions or the Quadrature by Expansion (QBX) technique in higher dimensions [7], resulting in a dense linear system where the matrix describes how the discretized source and target particles interact through the domain Green's function. In the numerical solver stage, an important and major computational cost in the GMRES or similar iterative methods is the efficient application of this matrix to a given vector representing the source distributions, which incurs an $\mathcal{O}(N^2)$ cost with a direct matrix-vector multiplication.

There exist several more efficient strategies to compute integral operators of the spatially variant domain Green's function efficiently. For simple geometries, for instance, the half-space or circles, one technique is to represent the domain Green's function as the sum of the free-space Green's function contributions from both the original source and some image points (the spatial variant properties are incorporated into the locations of the images). This approximation allows the direct application of existing free-space fast matrix vector multiplication algorithms specially designed for the free-space translation-invariant kernels, including the well-developed fast multipole method (FMM) packages in [8–11]. Representing works along this direction include the classical Kelvin image for the half-space problem (or circles) for the perfect conducting media [12], so the spatially variant domain Green's function simply consists of two free-space Coulomb potentials, one from the source charge and one from its image. In the case of dielectric inhomogeneity, such as a spherical cavity embedded in a dielectric medium, the reaction field from the media can also be approximated by a small number of image charges [13,14]. Unfortunately, for more complex geometry, the image approximations are extremely hard to derive or non-existent, and for a few special cases including the multi-layered media, the domain Green's functions are customarily derived as Sommerfeld integral formulas using integral transformations. Even when the image approximation formulas are available (e.g., the two-layered media Helmholtz equation), a large number of images is usually required. In [15], to approximate the interaction of 6,400 particles described by the domain Green's function of the 2-D Helmholtz equation with half-space impedance boundary condition, a total of 1,122,960 additional images were introduced in a hybrid approach, which combines the image and Sommerfeld integral representations. Other efforts to speed up the computation of integral operator for layered media Green's functions include the inhomogeneous plane wave method [16], windowed Green's function method for layered-media [17], and cylindrical wave decomposition of the Green's function in 3-D and 2-D FMM [18]. Fast Fourier Transform (FFT) has also been used to speed up the solution of volume integral equations in layered media by using the fact that the domain Green's function involves translation invariant convolution in the two horizontal x and y directions while a correlation along the vertical z-direction [19,20]. Both the convolutions and correlation can be implemented with FFTs. However, the FFT approach is usually used when the source distribution density is almost uniform in space and an interpolation to a regular Cartesian mesh is also needed when the source locations are random. The H-FMM method developed in this paper is designed for any type of source distribution such as sources on lower dimensional surfaces or curves or randomly objects in different parts of the space. Moreover, the H-FMM method has a complexity of $\mathcal{O}(N)$ for static or low frequency wave problems while FFT based methods' complexity is $\mathcal{O}(N \log N)$. Another approach is to compress the matrix describing the domain Green's function interactions directly using the fast direct solvers (FDS) [21,22] or closely related $\mathcal{H}$-matrix theory [23,24], where the low-rank structures of the sub-matrices are derived and processed recursively on a hierarchical tree structure using purely numerical linear algebra techniques. However, evaluating the domain Green's functions (entries in the matrix) involves very expensive computation of the Sommerfeld type integrals, and the compression stage of the FDS is expensive and memory intensive. It is worth mentioning that the FMM, FDS, and $\mathcal{H}$-matrix are all hierarchical algorithms that recursively compress the information in a system to low-rank or low-dimensional forms and transmit the compressed information non-locally on a hierarchical tree structure. In this paper, we apply this hierarchical algorithm design approach to multi-layered media domain Green's functions and present a new hierarchical algorithm for evaluating the spatially variant domain Green's function interactions. Our algorithm shares many common features with FMM and FDS algorithms, especially in the information transmission patterns on the tree structure: the compressed representations are transmitted through an upward pass from leaf to parent nodes on a hierarchical tree structure, collected by interacting nodes and stored as local expansions, and then transmitted to the children nodes in a downward pass. However, compared with the free-space FMM and domain Green's function FDS, the new algorithm has the following unique features: (a) It considers the domain Green's function (unlike the free-space FMM), but doesn't require the entry-wise function evaluation (unlike FDS); (b) It compresses the free-space Green's function (unlike FDS) to collect domain Green's function far-field contributions from children to parents in the upward pass. Direct compression of the domain Green's function is unnecessary (unlike FDS), but can be recovered from the free-space Green's function compression and Sommerfeld integral representation of the domain Green's function analytically; and (c) The multipole-to-local translation is heterogeneous (unlike the free-space FMM), and the translation operator can be derived analytically and computed efficiently on-the-fly using the Sommerfeld representation (unlike FDS). These attractive features imply that the new algorithm can be more efficient when simulating waves in layered media.

In this paper, we will focus on the case of a 2-D half-space (two-layered) problem where the domain Green's function can be explicitly represented with the Sommerfeld integrals or complex line images. The complex line image representation intuitively reveals how the compression of the interaction matrix can be performed analytically on a transformed matrix which only involves the free-space Green's function, and provides rigorous error analysis using available analytical results from the classical free-space FMM. As the compressed representation separates the spatially variant components and spatially invariant free-space kernels in the domain Green's function, both the multipole-to-multipole and local-to-local translations from the existing free-space Helmholtz FMM algorithm can be easily adapted. Unlike the classical spatially invariant FMM algorithm, all the spatially variant information are collected in the multipole-to-local translations and the new

algorithm becomes spatially variant. We refer to this new algorithm as the *Heterogeneous FMM* (H-FMM) due to the heterogeneous nature of the multipole-to-local translations and the use of the free-space Green's function and similar translations on the hierarchical tree structure from the classical FMM. We present the algorithm structure and demonstrate its accuracy and efficiency by comparing with the hybrid method in Ref. [15] for handling inhomogeneous media.

The rest of the paper is organized as follows. In Sec. 2, we present both the complex line image and Sommerfeld integral representations of the free-space and domain Green's functions for the 2-D Helmholtz equation with half-space impedance boundary condition. In Sec. 3, we present the hierarchical algorithm for the efficient evaluation of the spatially variant domain Green's function interactions for the two-layered case with impedance boundary conditions. We will discuss the hierarchical tree structure, compression of the complex image representations as multipole expansions, compression of the local interactions to allow more efficient evaluations of the integrals, adaptation of the spatially invariant multipole-to-multipole and local-to-local translations from existing free-space FMM, analytical formulas for the heterogeneous multipole-to-local translations and their efficient evaluations, and algorithm structures and some implementation details. Numerical results are presented in Sec. 4 to demonstrate the algorithm accuracy and efficiency in low frequency. Finally, we summarize our results in Sec. 5 and outline future work.

2. 2-D Helmholtz equation in impedance half-space

We present both the *complex line image* and *Sommerfeld integral representations* of the free-space and domain Green's functions for the 2-D Helmholtz equation in half-space with an impedance boundary condition.

2.1. Free-space Green's function

Consider the 2-D Helmholtz equation in free-space

$$(\Delta + k^2)u(\mathbf{x}) = 0$$

with the Sommerfeld radiation condition at infinity

$$\lim_{r\to\infty} \sqrt{r}\left(\frac{\partial}{\partial r}u(\mathbf{x}) - iku(\mathbf{x})\right) = 0,$$

where $\mathbf{x} = (x, y)$, $r = ||\mathbf{x}||$, k is the wave number, and $i = \sqrt{-1}$. Its Green's function is given by the 0th order Hankel function of the first kind as

$$g(\mathbf{x}, \mathbf{x}_0) = \frac{i}{4}H_0^{(1)}(k||\mathbf{x} - \mathbf{x}_0||) \tag{1}$$

which solves the equation

$$-(\Delta + k^2)g(\mathbf{x}, \mathbf{x}_0) = \delta(\mathbf{x} - \mathbf{x}_0) \tag{2}$$

with the Sommerfeld radiation condition

$$\lim_{r\to\infty} \sqrt{r}\left(\frac{\partial}{\partial r}g(\mathbf{x}, \mathbf{x}_0) - ikg(\mathbf{x}, \mathbf{x}_0)\right) = 0,$$

where δ is the 2-D Dirac delta function, $\mathbf{x}_0 = (x_0, y_0)$, and $r = ||\mathbf{x} - \mathbf{x}_0||$.

The free-space Green's function can be found in the frequency (spectral) domain by taking the Fourier transform of Eq. (2) in the x-direction and solving the resulting ordinary differential equations in the y-direction to give its spectral representation

$$g(\mathbf{x}, \mathbf{x}_0) = \frac{1}{4\pi}\int_{-\infty}^{\infty} \frac{e^{-\sqrt{\lambda^2-k^2}|y-y_0|}}{\sqrt{\lambda^2 - k^2}} e^{i\lambda(x-x_0)} d\lambda. \tag{3}$$

This representation is often referred to as the Sommerfeld identity, which can be separated into the propagating and evanescent modes for wave number variable $|\lambda| < k$ (propagating modes) and $|\lambda| > k$ (evanescent modes as $|y| \to \infty$), respectively, to arrive at the following form after some changes of variables

$$\begin{aligned} g(\mathbf{x}, \mathbf{x}_0) =& g(\mathbf{x}, \mathbf{x}_0)_{prop} + g(\mathbf{x}, \mathbf{x}_0)_{evan} \\ =& \frac{i}{4\pi}\int_0^{\pi} e^{ik(|y-y_0|\sin\theta - (x-x_0)\cos\theta)} d\theta + \frac{1}{4\pi}\int_0^{\infty} \frac{e^{-t|y-y_0|}}{\sqrt{t^2+k^2}}\left(e^{i\sqrt{t^2+k^2}(x-x_0)} + e^{-i\sqrt{t^2+k^2}(x-x_0)}\right) dt \end{aligned} \tag{4}$$

for $|y - y_0| > 0$ [25].

The free-space Green's function is commonly used in the potential theory, where solutions of the Helmholtz equation are represented as combinations of volume and/or layer potentials defined as the convolution of the Green's function or its derivatives with certain density functions either over the volume or surface area of a given object. Theoretical properties of the free-space Green's function and corresponding potentials are well-established in existing literature [26,27], and their efficient evaluations can be carried out using fast algorithms such as the well-developed fast multipole method for the Helmholtz equation [8,28].

2.2. Domain Green's function for two-layered media

In layered media, it is usually possible to derive the spatially variant domain Green's function analytically either using the method of images (complex image representation) for some simple setting, or applying the integral transforms (e.g., Laplace and Fourier transforms) for more complex multi-layer setting to have the spectral domain representation (Sommerfeld integral representation). In this subsection, we focus on the 2-D half-space Helmholtz equation with the impedance boundary condition

$$\frac{\partial u}{\partial \mathbf{n}} - i\alpha u = 0 \tag{5}$$

which is imposed on the interface defined by $y = 0$, and present the complex image and Sommerfeld integral representations from existing literature (e.g., see [29]).

Complex Image Representation. Let $u_{\mathbf{x}_0}(\mathbf{x})$ be the domain Green's function at $\mathbf{x}$ due to a point source located at $\mathbf{x}_0$. Then, it is decomposed as the sum of the free-space interaction of the source and target points that is the free-space Green's function $g(\mathbf{x}, \mathbf{x}_0)$ and contribution from a scattered field $u^s_{\mathbf{x}_0}(\mathbf{x})$, namely,

$$u_{\mathbf{x}_0}(\mathbf{x}) = g(\mathbf{x}, \mathbf{x}_0) + u^s_{\mathbf{x}_0}(\mathbf{x}). \tag{6}$$

The $u^s_{\mathbf{x}_0}(\mathbf{x})$ can be explicitly represented in the two-layered media as complex image contributions of the free-space kernel as

$$u^s_{\mathbf{x}_0}(\mathbf{x}) = \int_0^\infty g(\mathbf{x}, \mathbf{x}_0^{im} - s\hat{\mathbf{y}})\tau(s)ds, \tag{7}$$

where $\mathbf{x}_0^{im} = (x_0, -y_0)$ is the image of the source point $\mathbf{x}_0$, $\hat{\mathbf{y}} = (0, 1)$, and $\tau(s)$ is the complex image charge density distribution. By applying the impedance boundary condition, the image function $\tau(s)$ can be explicitly found as (see [15])

$$\tau(s) = \delta(s) + \mu(s), \quad s > 0, \tag{8}$$

where a point image is indicated by the Dirac delta distribution $\delta(s)$ and a line image $\mu(s)$ is given by

$$\mu(s) = 2i\alpha e^{i\alpha \cdot s}. \tag{9}$$

As a result, we have

$$u^s_{\mathbf{x}_0}(\mathbf{x}) = g(\mathbf{x}, \mathbf{x}_0^{im}) + \int_0^\infty g(\mathbf{x}, \mathbf{x}_0^{im} - s\hat{\mathbf{y}})\mu(s)ds, \tag{10}$$

where the first term on the right hand side represents the contribution from the point-image source, and the second term represents the contributions from the line-images. Therefore, the domain Green's function $u_{\mathbf{x}_0}(\mathbf{x})$ for the half-space Helmholtz equation with impedance boundary condition can be represented in terms of the free-space Green's function as

$$u_{\mathbf{x}_0}(\mathbf{x}) = g(\mathbf{x}, \mathbf{x}_0) + \left(g(\mathbf{x}, \mathbf{x}_0^{im}) + \int_0^\infty g(\mathbf{x}, \mathbf{x}_0^{im} - s\hat{\mathbf{y}})\mu(s)ds \right). \tag{11}$$

Sommerfeld Integral Representation. The scattered field in (10) involves an integration of an oscillatory line image density $\mu(s) = 2i\alpha e^{i\alpha \cdot s}$, which cannot be handled efficiently with numerical quadratures directly as in the case for the Laplace equation in [14]. However, using the Sommerfeld identity for $g(\mathbf{x}, \mathbf{x}_0)$ in Eq. (3), we can resolve this difficulty with an analytic integration of the s variable as follows:

$$\begin{aligned}
&\int_0^\infty g(\mathbf{x}, \mathbf{x}_0^{im} - s\hat{\mathbf{y}}) e^{i\alpha\cdot s} ds \\
&= \int_0^\infty \left[\frac{1}{4\pi} \int_{-\infty}^{\infty} \frac{e^{-\sqrt{\lambda^2-k^2}|y+y_0+s|}}{\sqrt{\lambda^2-k^2}} e^{i\lambda(x-x_0)} d\lambda \right] e^{i\alpha\cdot s} ds \\
&= \frac{1}{4\pi} \int_{-\infty}^{\infty} \frac{e^{-\sqrt{\lambda^2-k^2}(y+y_0)} e^{i\lambda(x-x_0)}}{\sqrt{\lambda^2-k^2}} \left[\int_0^\infty e^{-\sqrt{\lambda^2-k^2}s} e^{i\alpha\cdot s} ds \right] d\lambda \\
&= \frac{1}{4\pi} \int_{-\infty}^{\infty} \frac{e^{-\sqrt{\lambda^2-k^2}(y+y_0)} e^{i\lambda(x-x_0)}}{\sqrt{\lambda^2-k^2}} \frac{1}{\sqrt{\lambda^2-k^2} - i\alpha} d\lambda. \qquad (12)
\end{aligned}$$

Plugging Eqs. (12) and (3) into Eq. (11), we obtain the following spectral domain representation for the scattered field (assume $y > 0$)

$$u^s_{\mathbf{x}_0}(\mathbf{x}) = \frac{1}{4\pi} \int_{-\infty}^{\infty} \frac{e^{-\sqrt{\lambda^2-k^2}(y+y_0)}}{\sqrt{\lambda^2-k^2}} e^{i\lambda(x-x_0)} \frac{\sqrt{\lambda^2-k^2}+i\alpha}{\sqrt{\lambda^2-k^2}-i\alpha} d\lambda, \qquad (13)$$

or by defining

$$\hat{\sigma}(\lambda) = \frac{\sqrt{\lambda^2-k^2}+i\alpha}{\sqrt{\lambda^2-k^2}-i\alpha}, \qquad (14)$$

we have

$$u^s_{\mathbf{x}_0}(\mathbf{x}) = \frac{1}{4\pi} \int_{-\infty}^{\infty} \frac{e^{-\sqrt{\lambda^2-k^2}y}}{\sqrt{\lambda^2-k^2}} e^{i\lambda x} e^{-\sqrt{\lambda^2-k^2}y_0} e^{-i\lambda x_0} \hat{\sigma}(\lambda) d\lambda \qquad (15)$$

where $\hat{\sigma}(\lambda)$ is independent of $\mathbf{x}$ and $\mathbf{x}_0$.

Moreover, the Sommerfeld representation of the scattering field in (15) will be used eventually to extend the algorithm developed for two-layered media in this paper to multiple-layered media.

2.3. Domain Green's function in integral equation methods

In most integral equation formulations of the Helmholtz equation, unlike the translation invariant free-space Green's function that only depends on the distance of $\mathbf{x}$ and $\mathbf{x}_0$, the domain Green's function for general complex geometry brings complications for being a two variable function and its values are simply no longer translation invariant but spatially variant. As a result, the computation and evaluation of the domain Green's function are more expensive than finding the solution of the original differential equation. There are a few exceptions, including the simulation of the layered-media Helmholtz equation where the interface or boundary is infinite and flat. For such cases, if using the free-space Green's function, the resulting potentials will involve the evaluations of integrals (potentials) over infinite interfaces. However, due to the radial symmetry, one can analytically derive the spatially variant domain Green's function, in the form of a Sommerfeld integral representation using integral transformations such as the Laplace and Fourier transforms.

There are many advantages by using the domain Green's function in forming the integral equation method (IEM) for the multi-layered media problem, for instance, the interface conditions are naturally enforced by the domain Green's function and no unknowns are necessary on the layer interfaces. However, the numerical solution of the integral equation poses many challenges and is still an active research topic. In addition to problems common to all integral equation approaches such as the design of high order quadrature and derivation of well-conditioned systems, the IEM for layered media using the domain Green's function has its specific challenges. In particular, the evaluation of the domain Green's function interactions with large number of source and target points is expensive for either the complex image representation [15], or the Sommerfeld integral, or even the optimized hybrid representations. This implies that explicitly constructing the discretized interaction matrix is also expensive, and therefore matrix compression using the FDS will be costly where purely numerical linear algebra techniques are applied. This paper focuses on the fast application of the domain Green's function to a given density function $\rho(\mathbf{x}_0)$ as in

$$\phi(\mathbf{x}) = \int u_{\mathbf{x}_0}(\mathbf{x}) \rho(x_0) d\mathbf{x}_0, \qquad (16)$$

where the integral either represents a volume potential or a surface layer potential. After discretization, the resulting linear algebra question becomes how to efficiently calculate the matrix-vector multiplication of $A\mathbf{v}$ where entries in the matrix A are given by the domain Green's function $[A_{i,j}] = u_{\mathbf{x}_j}(\mathbf{x}_i)$. The main results of this paper include (a) the analysis-based low-rank compression of the matrix A, which is not directly performed on the matrix itself as in the FDS methods, but on a closely related matrix after certain transformations; (b) how the compressed representations can be transmitted through the hierarchical tree structure using analysis-based translation operators, and whenever possible, utilizing existing translation operators for the free-space kernels; and (c) the selected compression and translation strategies allow the implementation of a H-FMM algorithm for the layered media by an easy adaptation of existing free-space FMM codes.

3. Algorithm for two-layered media

In this section, we present the technical details of a fast hierarchical algorithm for the two-layered media domain Green's function. The algorithm is similar in structure to that of FMM and the compression stage of FDS, and is developed by considering the design philosophy of the hierarchical modeling technique. This technique identifies any low-rank, or low-dimensional, or other compact features in a given system, recursively collects the compressed representations from children to parents, and transmits the information between different nodes on a hierarchical tree structure using properly compressed translation operators. It is worth mentioning that the resulting hierarchical models are often re-expressed as recursive algorithms, which can be easily interfaced with existing dynamical schedulers from High-Performance Computing (HPC) community for optimal parallel efficiency [30–32].

In addition to FMM and FDS, different aspects of the hierarchical modeling technique have been known and addressed by many researchers previously. Examples include the classical fast Fourier transform (FFT) [33] where the Halving Lemma shows how data can be compressed and the odd-even term splitting of the polynomials creates a hierarchical tree to allow recursively processing the compressed information efficiently; the multigrid method (MG) [34,35] where the hierarchical tree structure is formed via adaptively refining the computational domain, and data compression and transmission are performed using the relaxation (smoother) and projection (restriction) operators by analyzing the frequency domain behaviors of the error functions between different levels of the (adaptive) tree to effectively reduce the high frequency errors. When there are n terms (FFT) in the polynomial or n approximately uniformly distributed particles (MG or FMM), the depth of the hierarchical tree is normally $\mathcal{O}(\log n)$ and the number of tree nodes is approximately $\mathcal{O}(n)$. Therefore, if each level only requires $\mathcal{O}(n)$ operations (e.g., FFT), the algorithm complexity will be $\mathcal{O}(n \log n)$. If each tree node only requires a constant amount of operations (e.g. MG or FMM), the algorithm complexity will be asymptotically optimal $\mathcal{O}(n)$. In this section, we describe our algorithm following the design guidelines of the hierarchical modeling technique.

3.1. Adaptive hierarchical tree structure

Consider the Helmholtz equation in 2-D with half-space impedance boundary condition for the scattering of a finite-sized object with a complex geometry in the upper half plane $y > 0$. A surface integral equation can be derived to give the scattering solution as layer potentials through a convolution of the domain Green's function or its derivatives with some unknown density functions over the object's surface. We assume the surface is discretized into a number of particles via proper numerical integration techniques. In the hierarchical modeling technique, a spatial adaptive hierarchical tree is first generated. In our algorithm, the tree structure is identical to that in FMM or FDS and is generated by a recursive partition to divide the particle-occupant region into nested square boxes, where the root box is the smallest bounding box that contains the entire particle set. Without loss of generality, the root box is normalized to size 1 along each side. The root box is partitioned equally along each dimension. The partition continues recursively on the resulting box until the box contains no more than s particles, at which point it becomes a leaf node. Empty boxes encountered during partition are pruned off. In our implementation, the value s is chosen depending on the size of the particle set and other factors to allow an optimal performance.

3.2. Low rank compression

The low-rank structure for well-separated source and target points has been extensively studied for the free-space FMM and FDS algorithms. Consider N sources with strength q_j placed at $\mathbf{x}_j = (x_j, y_j)$ in a circle centered at $\mathbf{x}_c = (x_c, y_c)$ with radius R on top of the half-space, and suppose we are interested in the field at $\mathbf{x}$ due to all the source points given by

$$u^f(\mathbf{x}) = \sum_{j=1}^{N} q_j g(\mathbf{x}, \mathbf{x}_j), \tag{17}$$

where $g(\mathbf{x}, \mathbf{x}_j)$ is the free-space Green's function contribution. We say $\mathbf{x}$ is well-separated from the sources if the distance between $\mathbf{x}$ and the source circle center $\mathbf{x}_c$ is at least $3R$, see Fig. 1.

Free-space Green's function compression. Using Graf's addition theorem [36], the free-space Green's function interaction of well-separated sources $\mathbf{x}_j$ and target $\mathbf{x}$ can be compressed as a multipole expansion given by

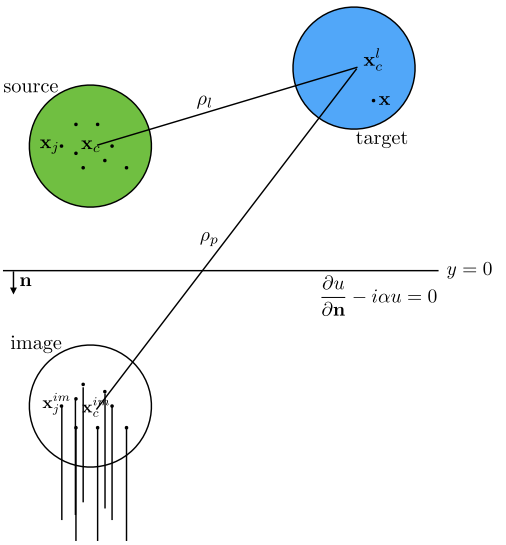

Fig. 1. Impedance half-space and notation. (For interpretation of the colors in the figure(s), the reader is referred to the web version of this article.)

$$u^f(\mathbf{x}) \approx \frac{i}{4} \sum_{p=-P}^{P} \alpha_p H_p^{(1)}(k|\mathbf{x} - \mathbf{x}_c|) e^{ip\theta_c}, \tag{18}$$

where

$$\alpha_p = \sum_{j=1}^{N} q_j e^{-ip\theta_j} J_p(k\rho_j), \tag{19}$$

θ_c is the polar angle of $\mathbf{x} - \mathbf{x}_c$, (ρ_j, θ_j) are the polar coordinates of the complex number $\mathbf{x}_j - \mathbf{x}_c$, J_p is the pth order Bessel function, and the number of terms P is a constant independent of the number of the sources N [37].

Domain Green's function compression: For the half-space problem with an impedance boundary condition, the field at $\mathbf{x}$ due to all the source points is

$$u(\mathbf{x}) = \sum_{j=1}^{N} q_j u_{\mathbf{x}_j}(\mathbf{x}) = \sum_{j=1}^{N} q_j g(\mathbf{x}, \mathbf{x}_j) + \sum_{j=1}^{N} q_j u^s_{\mathbf{x}_j}(\mathbf{x}). \tag{20}$$

As the first term on the right hand side represents the free-space Green's function interaction and is already compressed in Eq. (18), we focus on the compression of the second term representing the scattered field. When using the complex image representation, it can be compressed simply as follows:

$$\begin{aligned} u^s(\mathbf{x}) &= \sum_{j=1}^{N} q_j u^s_{\mathbf{x}_j}(\mathbf{x}) \\ &= \frac{i}{4} \sum_{j=1}^{N} q_j \left(H_0^{(1)}(k|\mathbf{x} - \mathbf{x}_j^{im}|) + \int_0^{\infty} H_0^{(1)}(k|\mathbf{x} - (\mathbf{x}_j^{im} - s\hat{\mathbf{y}})|) \mu(s) ds \right) \\ &\approx \frac{i}{4} \sum_{p=-P}^{P} \bar{\alpha}_p \left(H_p^{(1)}(k|\mathbf{x} - \mathbf{x}_c^{im}|) e^{ip\theta_{im}} + \int_0^{\infty} H_p^{(1)}(k|\mathbf{x} - (\mathbf{x}_c^{im} - s\hat{\mathbf{y}})|) e^{ip\hat{\theta}_{im}} \mu(s) ds \right) \end{aligned} \tag{21}$$

where $\mathbf{x}_j^{im} = (x_j, -y_j)$ are the coordinates of the point-image charge, $\bar{\alpha}_p$ is the complex conjugate of the free-space multipole coefficient α_p in Eq. (19) (see [15]), and θ_{im} and $\hat{\theta}_{im}$ are the polar angles of complex number $\mathbf{x} - \mathbf{x}_c^{im}$ and $\mathbf{x} - (\mathbf{x}_c^{im} - s\hat{\mathbf{y}})$, respectively. Therefore, the multipole expansion for both the original and image sources is

$$u(\mathbf{x}) \approx \frac{i}{4} \sum_{p=-P}^{P} \alpha_p H_p^{(1)}(k|\mathbf{x} - \mathbf{x}_c|) e^{ip\theta_c} + \frac{i}{4} \sum_{p=-P}^{P} \bar{\alpha}_p \left(H_p^{(1)}(k|\mathbf{x} - \mathbf{x}_c^{im}|) e^{ip\theta_{im}} \right.$$

$$+\int_0^\infty H_p^{(1)}(k|\mathbf{x}-(\mathbf{x}_c^{im}-s\hat{\mathbf{y}})|)e^{ip\hat{\theta}_{im}}\mu(s)ds\Big), \tag{22}$$

which is the key formula behind the H-FMM for layered media.

We emphasize that the number of terms P for the scattered field expansion is the same as the one in the free-space expansion for the same accuracy requirement. This can be rigorously justified by the observation that when the original sources $\mathbf{x}_j$ (in the green circle centered at $\mathbf{x}_c$) in Fig. 1 are well-separated from the target point $\mathbf{x}$ (in the blue circle centered at $\mathbf{x}_c^l$), all the corresponding point-images $\mathbf{x}_j^{im}$ (in the circle centered at $\mathbf{x}_c^{im}$) are also well-separated from $\mathbf{x}$, and this is true also for the set of line-images on the rays starting from $\mathbf{x}_c^{im}$ with the same s value.

Remark 1. Eq. (22) suggests that for the domain Green's function interactions, when the source and target clusters are well-separated, it is possible to only compress the translation invariant free-space Green's function using a P-term multipole expansion with coefficients α_p as in Eq. (18) for a prescribed accuracy requirement, and all other related information in Eq. (22) can be recovered from α_p to the same accuracy. Also, unlike the FDS, the compression of the domain Green's function is not performed directly on the matrix entries, but on another matrix after some spatially variant transformations implicitly described in Eq. (22), and these transformations involve the complex conjugation operator. Finally, as the compression is only on the free-space Green's function, deriving parent's compressed representation and corresponding error analysis are exactly the same as those in the classical FMM algorithms, where the multipole-to-multipole translation can be used without any modification. We therefore skip the details of this translation operator in this paper.

3.3. Translations on the hierarchical tree structure

We discuss how the compressed representations can be transmitted on the hierarchical tree structure in this section. As our selected multipole and local representations of the compressed domain Green's function are the same as those for the translation invariant free-space Green's function, existing multipole-to-multipole and local-to-local translations in the free-space FMM can be applied without any modification. We therefore focus on the multipole-to-local (M2L) translation operator, and study how the multipole expansion of the compressed domain Green's function can be converted to local expansions.

We start from the following well-known M2L translation operator for the free-space Green's function. Consider the same source points $\mathbf{x}_j$, $j=1,\cdots,N$ described in Fig. 1 and the compressed representation of the free-space kernel in Eq. (18). Then the free-space potential $u^f(\mathbf{x})$ can be translated to a local expansion centered at $\mathbf{x}_c^l$ using Graf's addition theorem as

$$u^f(\mathbf{x}) \approx \frac{i}{4}\sum_{p=-P}^{P}\beta_p^f J_p(k|\mathbf{x}-\mathbf{x}_c^l|)e^{ik\theta}, \tag{23}$$

where the coefficients are

$$\beta_p^f = \sum_{m=-P}^{P}\alpha_m H_{m-p}^{(1)}(k\rho_l)e^{i(m-p)\theta_l}, \tag{24}$$

θ is the polar angle of $\mathbf{x}-\mathbf{x}_c^l$, and (ρ_l,θ_l) are the polar coordinates of $\mathbf{x}_c^l-\mathbf{x}_c$ [37]. Because the complex image representation of the domain Green's function is given in terms of the free-space Green's function, we can therefore plug the free-space M2L translation formula in the compressed image representation of the scattered field

$$u^s(\mathbf{x}) \approx \frac{i}{4}\sum_{p=-P}^{P}\bar{\alpha}_p\Big(H_p^{(1)}(k|\mathbf{x}-\mathbf{x}_c^{im}|)e^{ip\theta_{im}} + \int_0^\infty H_p^{(1)}(k|\mathbf{x}-(\mathbf{x}_c^{im}-s\hat{\mathbf{y}})|)\mu(s)e^{ip\hat{\theta}_{im}}ds\Big), \tag{25}$$

to derive its local expansion given by

$$\begin{aligned} u^s(\mathbf{x}) &= \frac{i}{4}\sum_{p=-P}^{P}\sum_{m=-p}^{p}\bar{\alpha}_m\Big(H_{m-p}^{(1)}(k\tilde{\rho}_{im})J_p(k|\mathbf{x}-\mathbf{x}_c^l|)e^{i(m-p)\tilde{\theta}_{im}}e^{ip\theta} \\ &\quad + \int_0^\infty H_{m-p}^{(1)}(k\hat{\tilde{\rho}}_{im})J_p(k|\mathbf{x}-\mathbf{x}_c^l|)e^{i(m-p)\hat{\tilde{\theta}}_{im}}\mu(s)e^{ip\theta}ds\Big) \\ &= \frac{i}{4}\sum_{p=-P}^{P}\beta_p^s J_p(k|\mathbf{x}-\mathbf{x}_c^l|)e^{ip\theta}, \end{aligned} \tag{26}$$

where the local expansion coefficients are given by

$$\beta_p^s = \sum_{m=-p}^{p} \bar{\alpha}_m \left(H_{m-p}^{(1)}(k\tilde{\rho}_{im}) e^{i(m-p)\tilde{\theta}_{im}} + \int_0^\infty H_{m-p}^{(1)}(k\hat{\tilde{\rho}}_{im}) e^{i(m-p)\hat{\tilde{\theta}}_{im}} \mu(s) ds \right), \tag{27}$$

θ is the polar angle of $\mathbf{x} - \mathbf{x}_c^l$, and $(\tilde{\rho}_{im}, \tilde{\theta}_{im})$ and $(\hat{\tilde{\rho}}_{im}, \hat{\tilde{\theta}}_{im})$ are the polar coordinates of $\mathbf{x}_c^l - \mathbf{x}_c^{im}$ and $\mathbf{x}_c^l - (\mathbf{x}_c^{im} - s\hat{\mathbf{y}})$, respectively.

The local expansion for $u(\mathbf{x})$ is simply the sum of the free-space Green's function and scattered field local expansions. As the translation operator from the compressed multipole coefficients $\{\alpha_p\}$ to the local coefficients $\{\beta_p^s\}$ involves the complex conjugate operator, for notation reasons, instead of combining the free-space with the complex image contributions in one single translation, we only construct the mapping matrix A for the scattered field,

$$\beta_p^s = \sum_{m=-p}^{p} A_{p,m} \bar{\alpha}_m, \tag{28}$$

where

$$A_{p,m} = \left(H_{m-p}^{(1)}(k\tilde{\rho}_{im}) e^{i(m-p)\tilde{\theta}_{im}} + \int_0^\infty H_{m-p}^{(1)}(k\hat{\tilde{\rho}}_{im}) e^{i(m-p)\hat{\tilde{\theta}}_{im}} \mu(s) ds \right). \tag{29}$$

Notice that the integrand in Eq. (29) is highly oscillatory for large s and its numerical computation usually requires special treatment. Here, using

$$H_n^{(1)}(k\rho) e^{in\theta} = \left(-\frac{1}{k}\right)^n \left(\frac{\partial}{\partial x} + i\frac{\partial}{\partial y}\right)^n H_0^{(1)}(k\rho)$$

and the Sommerfeld representation of $H_0(k\rho)$ given in Eq. (3), the nth order Hankel function can be expressed as

$$H_n^{(1)}(k\rho) e^{in\theta} = \frac{(-i)^n}{i\pi} \int_{-\infty}^{\infty} \frac{e^{-\sqrt{\lambda^2-k^2}y}}{\sqrt{\lambda^2-k^2}} e^{i\lambda x} \left(\frac{\lambda - \sqrt{\lambda^2-k^2}}{k}\right)^n d\lambda, \quad y > 0 \tag{30}$$

where (ρ, θ) are the polar coordinates of the complex number $x + iy$. Then, the first term $H_{m-p}(k\tilde{\rho}_{im}) e^{i(m-p)\tilde{\theta}_{im}}$ in Eq. (29) is rewritten in terms of the *plane wave* expansion

$$H_{m-p}^{(1)}(k\tilde{\rho}_{im}) e^{i(m-p)\tilde{\theta}_{im}} = \frac{i^{m-p}}{\pi} \int_0^\pi e^{ik(y\sin\tau - x\cos\tau)} e^{-i(m-p)\theta} d\tau + \frac{(-i)^{m-p}}{i\pi} \int_0^\infty \frac{e^{-ty}}{\sqrt{t^2+k^2}} K(t) dt, \tag{31}$$

where (x, y) are the Cartesian coordinates of $(\tilde{\rho}_{im}, \tilde{\theta}_{im})$ and

$$K(t) = e^{i\sqrt{t^2+k^2}x} \left(\frac{\sqrt{t^2+k^2} - t}{k}\right)^{m-p} + e^{-i\sqrt{t^2+k^2}x} \left(\frac{-\sqrt{t^2+k^2} - t}{k}\right)^{m-p}$$

for $y > 0$. This plane wave representation was also used to diagonalize the M2L translation operator in the new version of the low frequency FMM for the free-space Green's function in [25]. We skip the similar formula for $H_{m-p}(k\hat{\tilde{\rho}}_{im}) e^{i(m-p)\hat{\tilde{\theta}}_{im}}$, and present the translation matrix explicitly in terms of propagating and evanescent parts as

$$\begin{aligned} A_{p,m} = & \frac{i^{m-p}}{\pi} \int_0^\pi e^{ik(y\sin\tau - x\cos\tau)} e^{-i(m-p)\theta} \left(\frac{k\sin(\tau) - \alpha}{k\sin(\tau) + \alpha}\right) d\tau \\ & + \frac{(-i)^{m-p}}{i\pi} \int_0^\infty \frac{e^{-ty}}{\sqrt{t^2+k^2}} \left(e^{i\sqrt{t^2+k^2}x} \left(\frac{\sqrt{t^2+k^2} - t}{k}\right)^{m-p} + e^{-i\sqrt{t^2+k^2}x} \left(\frac{-\sqrt{t^2+k^2} - t}{k}\right)^{m-p} \right) \left(\frac{t + i\alpha}{t - i\alpha}\right) dt \end{aligned} \tag{32}$$

after integrating the s variable analytically. In the numerical evaluation, the integral of the propagating term over a finite interval can be computed with high order Gauss quadrature and the evanescent term can be evaluated using the generalized Laguerre quadrature with weight function $t^n e^{-t}$.

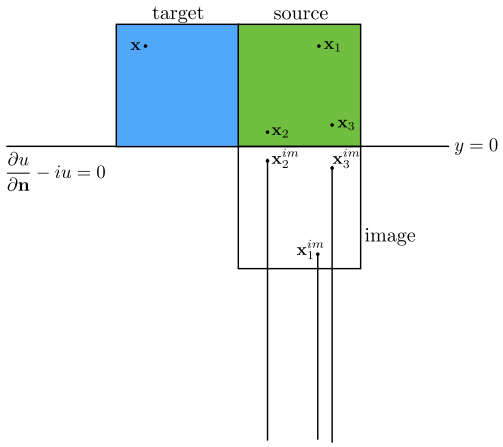

Fig. 2. Images are separated to near- and far-field by choosing appropriate C.

The translation matrix A in Eq. (32) has several special features. Unlike in the classical FMM algorithms, it depends on the x and y and is therefore spatially variant. However, for the fixed x and y, it is not a two variable function of m and p and only depends on $m - p$. In the numerical implementation, the matrix can be either computed on-the-fly, or precomputed and stored. We can estimate the required storage in the algorithm as follows: the translation operators $A_{p,m}$ are needed for all levels of the tree. For a fixed box, translation matrix consists of $4p$ complex values (as it is only a function of $m - p$) and there is a total of no more than $7 \cdot 7 = 49$ surrounding boxes representing the well-separated "receiving" boxes. For the two-layered media case, the matrix also depends on the y-coordinate of the center of the box as the translation operator takes different values as their images change. Thus, we can conclude that at tree level l, there are 2^l different values of y-coordinates, and for each y-coordinate 49 possible well-separated boxes that requires $4p$ complex values. Therefore, the total required storage for a system with L-levels is approximately $(2^{L+1} \cdot 49 \cdot 4p) \cdot 16$ bytes, which is very small compared with the required storage for different expansions.

Remark 2. It is also possible to derive the translation matrix in Eq. (28) directly using the Sommerfeld integral representation. This is in fact the key step to generalize the H-FMM to multi-layered media domain Green's function cases where only the Sommerfeld representation is available and the image representation is too complex to derive. Research results along this direction will be presented in a subsequent paper for multi-layered media in higher dimensions.

3.4. Accelerated evaluation of local direct interactions

We consider the submatrix representing the local direct interactions in this section. For a source box with N_b particles located at $\{\mathbf{x}_j\}_{j=1}^{N_b}$, its domain Green's function contribution to a target point $\mathbf{x}$ in a neighboring box is defined as

$$u^d(\mathbf{x}) = \frac{i}{4}\sum_{j=1}^{N_b} q_j H_0^{(1)}(k|\mathbf{x}-\mathbf{x}_j|) + \frac{i}{4}\sum_{j=1}^{N_b} q_j \left(H_0^{(1)}(k|\mathbf{x}-\mathbf{x}_j^{im}|) + \int_0^{\infty} H_0^{(1)}(k|\mathbf{x}-(\mathbf{x}_j^{im} - s\hat{\mathbf{y}})|)\mu(s)ds \right). \tag{33}$$

This formula shows the entries in one row of the submatrix. Further compression of the submatrix is usually impossible as it is not low-rank. However, it is still possible to take advantage of the compressed scattered field representations of the domain Green's function given in Eq. (21), so the entries in the submatrices can be evaluated more efficiently.

In Fig. 2, we show a source box sitting next to a target box. In this figure, notice that most of the line-images are well-separated from the target box. We can therefore choose an appropriate constant C and cut the line-images into two parts: those that are well-separated from the target box and those that are not. The evaluation of Eq. (33) can be divided as $u^d(\mathbf{x}) = I + II$, where

$$I = \frac{i}{4}\sum_{j=1}^{N_b} q_j H_0^{(1)}(k|\mathbf{x}-\mathbf{x}_j|) + q_j \left(H_0^{(1)}(k|\mathbf{x}-\mathbf{x}_j^{im}|) + \int_0^{C} H_0^{(1)}(k|\mathbf{x}-(\mathbf{x}_j^{im} - s\hat{\mathbf{y}})|)\mu(s)ds \right), \tag{34}$$

$$II = \frac{i}{4}\sum_{j=1}^{N_b} q_j \int_C^{\infty} H_0^{(1)}(k|\mathbf{x}-(\mathbf{x}_j^{im} - s\hat{\mathbf{y}})|)\mu(s)ds. \tag{35}$$

The first summation I is computed directly using high order quadrature for the finite size integral. For the second summation II, because $\mathbf{x}_j^{im} - s\hat{\mathbf{y}}$ is well-separated from the target point, the computation can be accelerated using the available source box multipole expansion as follows.

$$\begin{aligned} II &= \frac{i}{4}\sum_{j=1}^{N_b} q_j \int_C^{\infty} H_0^{(1)}(k|\mathbf{x} - (\mathbf{x}_j^{im} - s\hat{\mathbf{y}})|)\mu(s)ds \\ &= \frac{i}{4}\int_C^{\infty} \sum_{m=-P}^{P} \bar{\alpha}_m H_m^{(1)}(k|\mathbf{x} - (\mathbf{x}_c^{im} - s\hat{\mathbf{y}})|)e^{im\hat{\theta}_{im}}\mu(s)ds \\ &= \frac{i}{4}\int_C^{\infty} \sum_{m=-P}^{P} \bar{\alpha}_m \sum_{n=-\infty}^{\infty} H_{m-n}^{(1)}(k\tilde{\rho}_{im})e^{i(m-n)\hat{\tilde{\theta}}_{im}} J_n(k|\mathbf{x} - \mathbf{x}_c^l|)e^{in\theta}\mu(s)ds \\ &= \frac{i}{4}\sum_{n=-\infty}^{\infty}\left(\sum_{m=-P}^{P} \bar{\alpha}_m \int_C^{\infty} H_{m-n}^{(1)}(k\tilde{\rho}_{im})e^{i(m-n)\hat{\tilde{\theta}}_{im}}\mu(s)ds\right) J_n(k|\mathbf{x} - \mathbf{x}_c^l|)e^{in\theta} \\ &\approx \frac{i}{4}\sum_{n=-P}^{P} L_n J_n(k|\mathbf{x} - \mathbf{x}_c^l|)e^{in\theta}, \end{aligned} \tag{36}$$

where

$$L_n = \sum_{m=-P}^{P} \bar{\alpha}_m \int_C^{\infty} H_{m-n}^{(1)}(k\tilde{\rho}_{im})e^{i(m-n)\hat{\tilde{\theta}}_{im}}\mu(s)ds = \sum_{m=-k}^{k} \bar{\alpha}_m B_{m,k}$$

and the translation matrix is given by

$$B_{m,k} = \int_C^{\infty} H_{m-n}^{(1)}(k\tilde{\rho}_{im})e^{i(m-n)\hat{\tilde{\theta}}_{im}}\mu(s)ds, \tag{37}$$

which can be evaluated efficiently using the same Sommerfeld integral representation based technique in Eq. (32) for deriving the spatially variant M2L translation operators.

In the hierarchical tree structure, most boxes are well-separated from the interface $y = 0$. This implies that $C = 0$ for most direct interactions of the source and target boxes, and the separation can be simplified as

$$I = \frac{i}{4}\sum_{j=1}^{N_b} q_j H_0^{(1)}(k|\mathbf{x} - \mathbf{x}_j|), \tag{38}$$

$$II = \frac{i}{4}\sum_{j=1}^{N_b} q_j \left(H_0^{(1)}(k|\mathbf{x} - \mathbf{x}_j^{im}|) + \int_0^{\infty} H_0^{(1)}(k|\mathbf{x} - (\mathbf{x}_j^{im} - s\hat{\mathbf{y}})|)\mu(s)ds\right), \tag{39}$$

where both the point- and line-image contributions belong to II. In this case, the corresponding translation operator becomes the same as in Eq. (32). In the numerical simulation, all the translation matrices can be either precomputed or computed on-the-fly using high order quadrature for the Sommerfeld integral representation.

The selected compression schemes and translations allow easy adaptation of existing fast multipole algorithms for computing the domain Green's function interactions of the 2-D half-space Helmholtz equation with impedance boundary condition. We present the pseudo-code of our algorithm in the following.

Heterogeneous 2-D FMM for Two-layered Media with Impedance Boundary Conditions

Step 1: Initialization
Generate an adaptive hierarchical tree structure and precompute tables.
Comment [L denotes the maximum refinement level in the adaptive tree determined by a prescribed number s representing the maximum allowed number of particles in a childless box.**]**

Step 2: Upward Pass

for $l = L, \ldots, 0$
  for all boxes j on level l
    if j is a leaf node
      form the *free-space* multipole expansion using Eq. (18).
    else
      form the *free-space* multipole expansion by merging children's expansions using the *free-space* multipole-to-multipole translation operator.
    endif
  end
end

Cost [All operations in this step are the same as those in the *free-space* FMM.**]**

Step 3: Downward Pass

for $l = 1, \ldots, L$
  for all boxes j on level l
    shift the local expansion of j's parent to j itself using the *free-space* local-to-local translation operator.
    collect interaction list contribution using the precomputed table and the multipole-to-local translation operator in Eq. (29).
  end
end

Cost [Using the precomputed table, the cost is expected to be the same as in the *free-space* FMM. Overhead operations are required when tables are computed on-the-fly.**]**

Step 4: Evaluate Local Expansions

for each leaf node (childless box)
  collect part II in Eq. (35) or (39) from neighboring (including self) boxes.
  evaluate the local expansion at each particle location.
end

Comment [At this point, for each target point, its far field contribution (including those from well-separated images) has been computed.**]**
Cost [Compared with the *free-space* FMM, additional translations are required to translate the multipole expansions of images to local expansions. The heterogeneous translation operators can be computed on-the-fly or precomputed. The amount of work is constant for each leaf node.**]**

Step 5: Local Direct Interactions

for $i = 1, \ldots, N$
  compute Part I in Eq. (34) or (38) of target point i with original and image sources in the neighboring boxes.
end

Cost [When the computational domain is well-separated from the boundary $y = 0$, this step only involves the evaluation of the *free-space* kernel in Eq. (38) and the cost is the same as the *free-space* FMM. When the computational domain is close to the boundary $y = 0$, a constant number of additional operations are required for each i in a very small subset of the particles to evaluate the near-field point- and line-image contributions from Part I in Eq. (35).**]**

In our current implementation, all the tables are precomputed using Mathematica requesting more than 20 digits accuracy. Compared with the original free-space FMM algorithm, the domain Green's function H-FMM only requires a small portion of additional cost, as demonstrated in the next section.

4. Numerical results

We present numerical results in this section to demonstrate the performance of the H-FMM algorithm for the two-layered media with the interface placed at $y = 0$, and set $\alpha = 1$ in the impedance boundary condition. We assume the

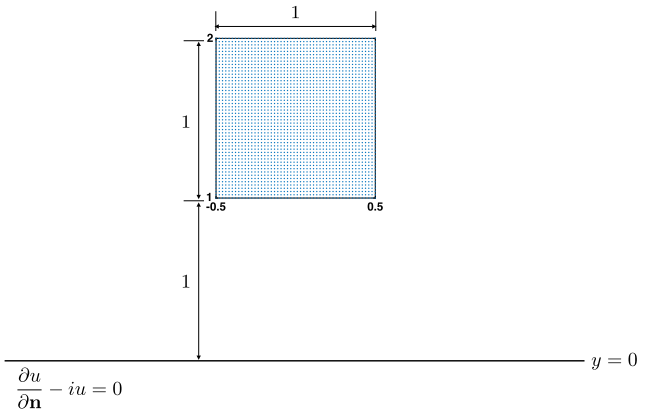

Fig. 3. Uniform distribution in a unit square on top of half-space.

Table 1
Accuracy results with different expansion terms for $k = 0.1$ and $k = 1$. Reference solution is computed with $p = 39$.

p	Error for $k = 0.1$	Error for $k = 1$
E_5	1.23×10^{-4}	1.43×10^{-4}
E_{10}	2.73×10^{-6}	3.81×10^{-6}
E_{20}	2.06×10^{-9}	2.85×10^{-9}
E_{30}	1.19×10^{-11}	1.65×10^{-11}

Table 2
CPU time (seconds) for different N using $p = 39$ and $k = 0.1$.

N	100	6400	10000	90000	360000	640000	810000	1000000
CPU time	0.01	0.67	1.19	10.92	46.58	100.85	116.03	135.05

source and target points are the same set of N particles located in a unit box centered at $(0, 1.5)$ as shown in Fig. 3. All the source strengths are set to 1. The code is written based on the free-space FMM in Refs. [8,38]. The numerical simulations are performed on a desktop with 3.7 GHz Xeon E5 processor and 32 GB RAM using the gcc compiler version 4.9.3. All the required translation tables are precomputed using Mathematica.

As the analytical solution is not available for this problem, we first check the algorithm accuracy by studying how the errors change as a function of the number of expansion terms p. We consider the example with $N = 100 \times 100$ particles uniformly distributed in the box. The random distribution resulted in almost the same data as the uniform distribution and they are not presented. A reference solution is computed using $p = 39$ (which should provide results with approximately 12-digit accuracy) and by setting $L = 3$ in the hierarchical tree structure. The H-FMM algorithm took about 1.19 seconds to derive the reference solutions. The accuracy results are presented in Table 1 for $p = 5, 10, 20, 30$ and wave numbers $k = 0.1$ and $k = 1$, respectively, where the error E_p using p terms in the expansion is defined as

$$E_p = \left(\frac{\sum_{j=1}^{M} |u_{39}(\mathbf{x}_j) - u_p(\mathbf{x}_j)|^2}{\sum_{j=1}^{M} |u_{39}(\mathbf{x}_j)|^2} \right)^{\frac{1}{2}}, \quad M = 10,000. \tag{40}$$

In Fig. 4(a), we plot how the error E_p decays as a function of p for $k = 0.1$. We see that the error dependency on the number of terms p to compress the domain Green's function is similar to that in existing FMM analysis for the free-space kernels.

We demonstrate the algorithm efficiency by presenting the CPU times in Table 2 for different numbers of source/target points N from 100 to $1,000,000$ for $k = 0.1$. Precomputation of the translation operator table with Mathematica took about 30 hours. In fact, this process can be completely parallelized. A log–log plot of the CPU time is also presented in Fig. 4(b), which clearly shows the linear scaling of the H-FMM algorithm. For comparisons, estimated results of direct computations (using CPU times for $N = 100$ and $6,400$) and the ideal linear scaling curve are also presented. As a comparison, in [15], the CPU time for computing the interactions of 6,400 particles is about 54.79 seconds, which is much slower as 1,122,960 additional images are introduced in the calculation. Similar experiments are performed for $k = 1$ and results are almost identical to that when $k = 0.1$ and are therefore omitted in this paper.

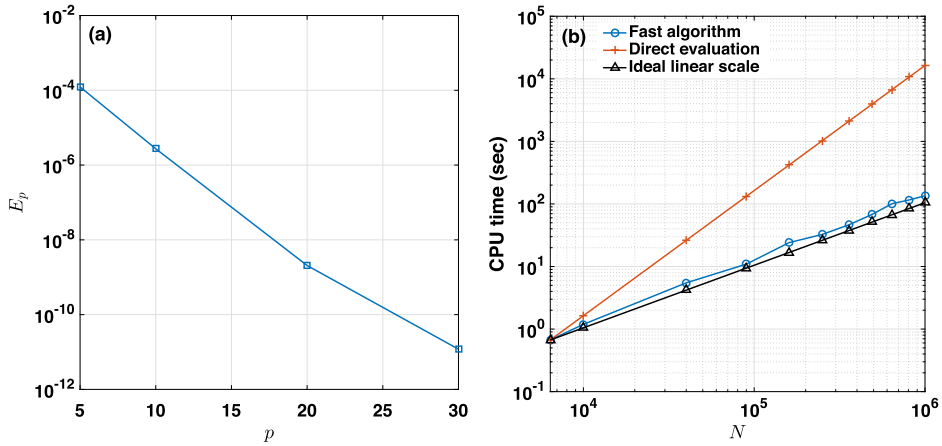

Fig. 4. (a) Convergence for $k = 0.1$ and $N = 10000$. (b) Linear CPU time scaling with $k = 0.1$ and $N = 6400, 10000, \cdots, 1000000$.

5. Conclusion and future work

We present a heterogeneous FMM for the efficient calculation of the discretized integral operator for the Helmholtz equation in two layer media with impedance boundary conditions. The two-layered media setting allows the use of the *complex line image* representations to compress the domain Green's function and to derive the translation operators analytically. Instead of compressing the interaction matrix directly, the *complex line image* representation intuitively reveals how a transformed matrix can be compressed through a procedure that only involves the free-space Green's function, and provides rigorous error bounds by using existing free-space FMM results. Unlike the fast direct solvers, the compression is performed analytically on a transformed matrix which allows the easy adaptation of existing free-space FMM packages. Also dissimilar to the classical FMM, the multipole-to-local translation operators are spatially variant, thus the translation operators in the FMM becomes heterogeneous. Numerical experiments show that the new hierarchical algorithm provides significant improvement over existing hybrid methods [15] in two-layered media settings.

This paper focuses on the intuitions through the two-layered media setting. In a subsequent paper, we will present a more general H-FMM for multi-layered media, based on the Sommerfeld integral representation as given in (15) when the image representation will be too complicated to use, addressing various issues including constructions and error analysis of compressions, translations for both the scalar Helmholtz equations in acoustic studies and the multi-layered media dyadic Green's function for the Maxwell's equations [39]. Finally, it is interesting to compare the analysis based compressions with those using purely numerical linear algebra techniques as in the fast direct solvers, to understand how the efficiencies of both compressions can be further improved. Research along these directions will also be explored in the future.

Acknowledgements

W. Cai was supported by US Army Research Office (Grant No. W911NF-17-1-0368) and US National Science Foundation (Grant No. DMS-1802143). M.H. Cho was supported by a grant from the Simons Foundation (No. 404499). Part of the work was finished when J. Huang was on a Senior Faculty Research and Scholarly Leave in fall 2017 sponsored by the University of North Carolina at Chapel Hill. Their supports are thankfully acknowledged.

References

[1] W.C. Chew, Waves and Fields in Inhomogeneous Media, vol. 522, IEEE Press, New York, 1995.
[2] J. Cui, W.C. Chew, Fast evaluation of Sommerfeld integrals for EM scattering and radiation by three-dimensional buried objects, IEEE Trans. Geosci. Remote Sens. 37 (2) (1999) 887–900.
[3] K.A. Michalski, D. Zheng, Electromagnetic scattering and radiation by surfaces of arbitrary shape in layered media. i. Theory, IEEE Trans. Antennas Propag. 38 (3) (1990) 335–344.
[4] D. Chen, M.H. Cho, W. Cai, Accurate and efficient Nyström volume integral equation method for electromagnetic scattering of 3-D meta materials in layered media, SIAM J. Sci. Comput. 40 (1) (2018) B259–B282.
[5] B.K. Alpert, Hybrid gauss-trapezoidal quadrature rules, SIAM J. Sci. Comput. 20 (5) (1999) 1551–1584.
[6] S. Kapur, V. Rokhlin, High-order corrected trapezoidal quadrature rules for singular functions, SIAM J. Numer. Anal. 34 (4) (1997) 1331–1356.
[7] A. Klöckner, A. Barnett, L. Greengard, M. O'Neil, Quadrature by expansion: a new method for the evaluation of layer potentials, J. Comput. Phys. 252 (2013) 332–349.
[8] M.H. Cho, W. Cai, A wideband fast multipole method for the two-dimensional complex helmholtz equation, Comput. Phys. Commun. 181 (12) (2010) 2086–2090.
[9] J. DeBuhr, B. Zhang, A. Tsueda, V. Tilstra-Smith, T. Sterling, Dashmm: dynamic adaptive system for hierarchical multipole methods, Commun. Comput. Phys. 20 (4) (2016) 1106–1126.
[10] Z. Gimbutas, L. Greengard, Computational software: simple fmm libraries for electrostatics, slow viscous flow, and frequency-domain wave propagation, Commun. Comput. Phys. 18 (02) (2015) 516–528.

[11] B. Zhang, J. Huang, N.P. Pitsianis, X. Sun, Rec fmm: recursive parallelization of the adaptive fast multipole method for coulomb and screened coulomb interactions, Commun. Comput. Phys. 20 (02) (2016) 534–550.
[12] J.C. Maxwell, A Treatise on Electricity and Magnetism, vol. 1, Clarendon Press, 1881.
[13] W. Cai, Computational Methods for Electromagnetic Phenomena: Electrostatics for Solvation, Scattering, and Electron Transport, Cambridge University Press, 2013.
[14] W. Cai, S. Deng, D. Jacobs, Extending the fast multipole method to charges inside or outside a dielectric sphere, J. Comput. Phys. 223 (2) (2007) 846–864.
[15] M. O'Neil, L. Greengard, A. Pataki, On the efficient representation of the half-space impedance Green's function for the Helmholtz equation, Wave Motion 51 (1) (2014) 1–13.
[16] B. Hu, W.C. Chew, Fast inhomogeneous plane wave algorithm for electromagnetic solutions in layered medium structures: two-dimensional case, Radio Sci. 35 (1) (2000) 31–43.
[17] O.P. Bruno, M. Lyon, C. Pérez-Arancibia, C. Turc, Windowed green function method for layered-media scattering, SIAM J. Appl. Math. 76 (5) (2016) 1871–1898.
[18] M.H. Cho, W. Cai, A parallel fast algorithm for computing the helmholtz integral operator in 3-d layered media, J. Comput. Phys. 231 (2012) 5910–5925.
[19] X. Millard, Q.H. Liu, A fast volume integral equation solver for electromagnetic scattering from large inhomogeneous objects in planarly layered media, IEEE Trans. Antennas Propag. 51 (9) (2003) 2393–2401.
[20] X. Millard, Q.H. Liu, Simulation of near-surface detection of objects in layered media by the BCGS-FFT method, IEEE Trans. Geosci. Remote Sens. 42 (2) (2004) 327–334.
[21] L. Greengard, D. Gueyffier, P.-G. Martinsson, V. Rokhlin, Fast direct solvers for integral equations in complex three-dimensional domains, Acta Numer. 18 (2009) 243–275.
[22] K.L. Ho, L. Greengard, A fast direct solver for structured linear systems by recursive skeletonization, SIAM J. Sci. Comput. 34 (5) (2012) A2507–A2532.
[23] W. Hackbusch, A sparse matrix arithmetic based on $\mathcal{H}$-matrices. part i: introduction to $\mathcal{H}$-matrices, Computing 62 (2) (1999) 89–108.
[24] W. Hackbusch, B.N. Khoromskij, A sparse $\mathcal{H}$-matrix arithmetic, Computing 64 (1) (2000) 21–47.
[25] L. Greengard, J. Huang, V. Rokhlin, S. Wandzura, Accelerating fast multipole methods for the helmholtz equation at low frequencies, IEEE Comput. Sci. Eng. 5 (3) (1998) 32–38.
[26] D. Colton, R. Kress, Integral Equation Methods in Scattering Theory, SIAM, 2013.
[27] R. Kress, V. Maz'ya, V. Kozlov, Linear Integral Equations, vol. 17, Springer, 1989.
[28] H. Cheng, W.Y. Crutchfield, Z. Gimbutas, L.F. Greengard, J.F. Ethridge, J. Huang, V. Rokhlin, N. Yarvin, J. Zhao, A wideband fast multipole method for the Helmholtz equation in three dimensions, J. Comput. Phys. 216 (1) (2006) 300–325.
[29] O.D. Kellogg, Foundations of Potential Theory, vol. 31, Springer Science & Business Media, 2012.
[30] High Performance ParallelX (HPX-5), https://hpx.crest.iu.edu/.
[31] R.D. Blumofe, C.F. Joerg, B.C. Kuszmaul, C.E. Leiserson, K.H. Randall, Y. Zhou, Cilk: an efficient multithreaded runtime system, J. Parallel Distrib. Comput. 37 (1) (1996) 55–69.
[32] M. Frigo, C.E. Leiserson, K.H. Randall, The Implementation of the cilk-5 Multithreaded Language, ACM SIGPLAN Not., vol. 33, ACM, 1998, pp. 212–223.
[33] J.W. Cooley, J.W. Tukey, An algorithm for the machine calculation of complex fourier series, Math. Comput. 19 (90) (1965) 297–301.
[34] A. Brandt, Multi-level adaptive solutions to boundary-value problems, Math. Comput. 31 (138) (1977) 333–390.
[35] W. Hackbusch, Multi-Grid Methods and Applications, vol. 4, Springer Science & Business Media, 2013.
[36] M. Abramowitz, I.A. Stegun, Handbook of Mathematical Functions with Formulas, Graphs, and Mathematical Tables, 10th edition, Dover, 1964.
[37] V. Rokhlin, Rapid solution of integral equations of scattering theory in two dimensions, J. Comput. Phys. 86 (2) (1990) 414–439.
[38] M.H. Cho, W. Cai, Revision of wfmm—a wideband fast multipole method for the two-dimensional complex Helmholtz equation, Comput. Phys. Commun. 183 (2) (2012) 446–447.
[39] M.H. Cho, W. Cai, Efficient and accurate computation of electric field dyadic green's function in layered media, J. Sci. Comput. 71 (3) (2017) 1319–1350.